Transport and scavenging of soluble gases in a deep convective cloud

JOURNAL OF GEOPHYSICAL RESEARCH, VOL. 105, NO. D17, PAGES 22,255–22,267, SEPTEMBER 16, 2000

Transport and scavenging of soluble gases in a deep convective cloud

Céline Mari

Laboratoire d'Aérologie, UMR CNRS/Université Paul Sabatier, Toulouse, France

Daniel J. Jacob

Division of Engineering and Applied Science, Harvard University, Cambridge, Massachusetts

Peter Bechtold

Laboratoire d'Aérologie, UMR CNRS/Université Paul Sabatier, Toulouse, France

Abstract. A one-dimensional entraining/detraining plume model is used to examine the transport and scavenging of soluble gases in tropical deep convection. The model is applied to a continental system observed over Brazil during the Trace and Atmospheric Chemistry Near the Equator-Atlantic (TRACE-A) TRACE-A aircraft campaign with outflows extending from 7 to 16 km altitude. Six gases are simulated: CO (inert tracer), CH_3OOH, CH_2O, H_2O_2, HNO_3 , and SO_2. Observed (simulated) convective enhancement factors (CEF) at 7-12 km altitude, representing the ratios of postconvective to preconvective mixing ratios, are 2.4 (1.9) for CO, 11 (9.5) for CH_3OOH, 2.9 (3.1) for CH_2O, 1.9 (1.2) for H_2O_2, and 0.8 (0.4) for HNO_3. Simulated scavenging efficiencies in the convective column are 5% for CH_3OOH, 23% for CH_2O, 66% for H_2O_2, 77% for HNO_3, and 28% for SO_2. The large CEF for CH_3OOH reflects its low solubility and its boundary layer enrichment relative to the upper troposphere. The Henry's law constant for CH_2O puts it at the threshold for efficient scavenging. Scavenging of SO_2 is limited by the rate of aqueous phase reaction with H_2O_2, as H_2O_2 is itself efficiently scavenged by Henry's law equilibrium; efficient scavenging of SO_2 requires unusually high cloud water pH (pH > 6) to enable fast aqueous phase oxidation by O_3. Both HNO_3 and H_2O_2 are efficiently scavenged in the lower (warm) part of the cloud, but H_2O_2 is released as the cloud freezes due to low retention efficiency during riming. Significant scavenging of H_2O_2 still takes place by cocondensation with ice in the glaciated cloud but is less efficient than in the warm cloud. Inefficient scavenging of H_2O_2 in glaciated clouds may explain the observation, in TRACE-A and elsewhere, that H_2O_2 is enhanced in deep convective outflows while HNO_3 is depleted. Model results indicate little direct transfer of air from the boundary layer to the cloud anvil in the convective plume, because of low-level detrainment in the warm cloud and high-level entrainment in the glaciated cloud. We find instead a convective ladder effect where midlevel outflow during the growing phase of the storm is reentrained into the convective plume as the storm matures.

1. Introduction

Deep convection in the tropics is a critical mechanism for transfer of air from the lower to the upper troposphere [*Cotton et al.*, 1995] with many important implications for atmospheric chemistry [*Prather and Jacob*, 1997]. Recent studies show that the upper troposphere is more photochemically active than previously thought due to the convective transport of radical precursors such as acetone, peroxides and aldehydes [*Singh et al.*, 1995; *McKeen et al.*, 1997; *Jaeglé et al.*, 1997; *Müller and Brasseur*, 1999]. Most of the NO_x in the upper troposphere is thought to originate from deep convective transport of NO_x and nitrate reservoirs produced by surface sources and lightning [*Lamarque et al.*, 1996; *Jacob et al.*, 1996; *Pickering et al.*, 1998; *Jaeglé et al.*, 1998]. Deep convective pumping of dimethylsulfide and SO_2 may drive efficient nucleation of sulfate aerosol in convective outflow [*Chatfield et Crutzen*, 1984; *Rodhe*, 1999]. Considerable precipitation takes

Paper number 2000JD900211.
0148-0227/00/2000JD900211$09.00

place in association with deep convection updrafts, and an unresolved issue is the degree to which precipitation scavenging suppresses the convective cloud venting of water-soluble gases [*Andronache et al.*, 1999; *Flossmann and Wobrock*, 1996; *Barth*, 1994]. We present here an analysis of this issue.

Our approach is based on a one-dimensional (1-D) entraining/detraining plume model (P. Bechtold et al., A mass flux convection scheme for regional and global models, submitted to *Quartely Journal of the Royal Meteorological Society*, 2000; hereinafter Bechtold et al., submitted manuscript, 2000) that has been designed to provide a deep convective parameterization for mesoscale and global-scale models. This model allows us to identify the key parameters controlling the vertical redistribution and scavenging of chemical species in a deep convective cloud. We examine here the fate of six different gases covering a range of solubility in water: (1) CO as an insoluble tracer of boundary layer pollution, (2) CH_2O, H_2O_2, CH_3OOH as precursors for the HO_x (HO_x = OH + peroxy radicals) family in the upper troposphere, (3) HNO_3 as a reservoir for NO_x , and (4) SO_2 as the precursor for sulfate aerosols.

We focus our analysis on a tropical continental convective case observed during the Transport and Atmospheric Chemistry Near the Equator-Atlantic (TRACE-A) aircraft experiment in September-October 1992. TRACE-A was designed to determine the role of biomass burning in causing the large-scale enhancement of tropospheric ozone observed over the south Atlantic basin in austral spring [*Fishman et al.*, 1996]. Two flights over eastern Brazil examined the convective pumping of biomass burning pollution to the upper troposphere. Of particular interest is flight 6, which provided vertical profiles of gases for both preconvective and postconvective conditions [*Pickering et al.*, 1996]. We use the data from flight 6 to constrain and evaluate our simulation of convective transport and scavenging of chemical species.

2. Model Description

2.1. One-Dimensional Entraining/Detraining Plume Model

A one-dimensional entraining/detraining plume model for wet convection (Bechtold et al., submitted manuscript, 2000) is used for this study. This model has been designed to provide a parameterization of wet convection in the mesoscale model Meso-NH [*Lafore et al.*, 1998]. Subgrid-scale fluxes through convective updrafts and mixing with the environment through entrainment and detrainment are diagnosed in terms of grid-scale thermodynamic and dynamic variables [*Bechtold et al.*, 2000; also Bechtold et al., submitted manuscript, 2000]. The formulation essentially follows the scheme of *Kain and Fritsch* [1990] which is an advanced version of the *Fritsch and Chappell* [1980] scheme. The model parameterizes a convective updraft plume balanced by a convective downdraft plume and by large-scale subsidence and includes entrainment and detrainment processes (Figure 1).

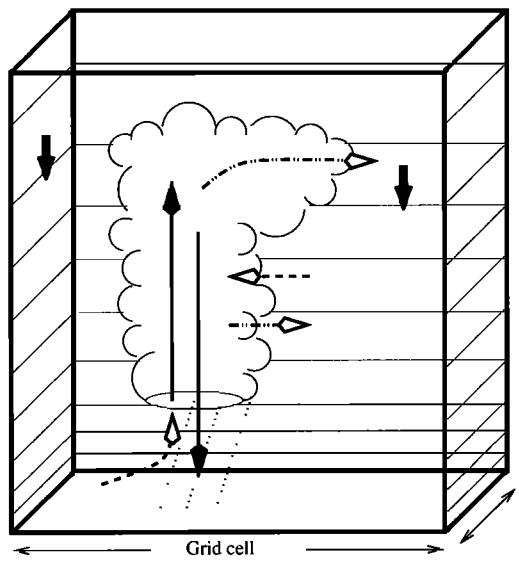

Figure 1. Schematic of the one-dimensional convective cloud model with updraft and downdraft regions (solid arrows), entrainment (open arrows with dashed tails), detrainment (open arrows with dash-dotted tails) and compensational large-scale subsidence (thick solid arrows)

In the present application the model is initialized with vertical profiles of temperature, water vapor and horizontal winds from the European Centre for Medium-Range Weather Forecasts (ECMWF) analysis at grid resolution 0.5° × 0.5°. Convection is triggered by convective instability and large-scale convergence. The net convective available potential energy (CAPE) is used to determine the updraft and downdraft air mass fluxes. At least 90% of the initial CAPE in the sounding must be removed by the calculated convective fluxes. Entrainment and detrainment refer to mass exchange between the updraft and the environment (Figure 1). The environment is defined as the grid scale of the ECMWF analysis and is also viewed here as the scale of the preconvective aircraft observations.

Entrainment and detrainment rates are computed following the scheme of *Kain and Fritsch* [1990] as a function of the buoyancy characteristics of individual updraft subparcels. The mixing between clouds and their environments occurs very near the periphery of clouds and generates subparcels containing various proportions of clear and cloudy air. Positively buoyant subparcels follow the cloudy updraft, entraining air from the environment, while negatively buoyant subparcels detrain to the environment.

At each model level, the rate δM_t ($\mathrm{kg\,s^{-1}}$), at which environmental air flows into the mixing region at the periphery of the updraft is expressed by

$$\delta M_t = 0.2 \frac{M_{u0}}{R_0} \delta z, \qquad (1)$$

where R_0 (1500 m) and M_{u0} ($\mathrm{kg\,s^{-1}}$) are the updraft radius and the mass flux at cloud base, and δz (m) is the vertical thickness of the level. The mass in this mixing region is then partitioned into entraining and detraining components. A mixing probability distribution, $f(x)$, is used to characterize the generation of mixed subparcels (where x is the fraction of environmental air in the mixed subparcels). Given this distribution, the rate at which updraft and environmental air mix into subparcels that are positively buoyant or negatively buoyant can be determined [*Kain and Fritsch*, 1990]. If the fractional amount of environmental mass that yields a neutrally buoyant mixture is labeled as χ_c, the entrainment rate, $M_\epsilon(\mathrm{kg\,m^{-1}\,s^{-1}})$ is given by

$$M_\epsilon = \frac{\delta M_t}{\delta z}\int_0^{\chi_c} x f(x)dx, \tag{2}$$

and the detrainment rate, $M_\delta(\mathrm{kg\,m^{-1}\,s^{-1}})$ is determined from

$$M_\delta = \frac{\delta M_t}{\delta z}\int_{\chi_c}^{1} (1-x) f(x)dx. \tag{3}$$

The updraft mass flux, M ($\mathrm{kg\,s^{-1}}$), changes through entrainment and detrainement according to

$$\frac{\partial M}{\partial z} = M_\epsilon - M_\delta. \tag{4}$$

An illustration is shown in Figure 2. The corresponding mass conservation equation for a conserved gas tracer of mixing ratio C in the convective plume is given by

$$\frac{\partial (MC)}{\partial z} = M_\epsilon \overline{C} - M_\delta C, \tag{5}$$

where $\overline{C}$ is the mixing ratio in the environmental air.

Entrainment is a critical process as it reduces the buoyancy of the cloudy air parcel and thus limits the depth of a convective plume triggered by low-altitude instability. It also has important chemical implications by supplying midlevel air to the updraft from which species can be pumped upward or scavenged. Conversely, detrainment allows the convective updraft to affect midlevel air and soluble species to escape complete scavenging.

At each model level, the liquid cloud and ice water condensate mixing ratios (respectively r_c and r_i) are deduced from the saturation vapor pressure of water and allowing a gradual linear glaciation of the cloud in the temperature interval betwen 268 and 248 K. It is assumed that cloud condensate is continuously removed from the updraft by precipitation processes. At each level in the updraft, precipitating particles are produced following the parameterization of *Ogura and Cho* [1973]:

$$\delta r_r + \delta r_s = (r_c + r_i)\,(1 - exp(-c_{pr}\frac{\delta z}{w})), \tag{6}$$

where c_{pr} (s^{-1}) is a local first-order rate constant for conversion of cloud condensate in liquid (r_c) and ice (r_i) phases to rain (δr_r) and snow (δr_s), and w denotes the updraft velocity. Values of c_{pr} in the litterature range from 0.001 $\mathrm{s^{-1}}$ [*Giorgi and Chameides*, 1986] to 0.01 $\mathrm{s^{-1}}$ [*Kain and Fritsch*, 1990]. In this work, c_{pr} is taken equal to 0.005 $\mathrm{s^{-1}}$ in the reference case, and sensitivity calculations are presented with c_{pr}=0.001, 0.01 and 0.02 $\mathrm{s^{-1}}$. For example, taking a vertical velocity of 20 $\mathrm{m\,s^{-1}}$ and c_{pr}=0.005 $\mathrm{s^{-1}}$ gives a scavenging efficiency of 22% $\mathrm{km^{-1}}$ for condensed water in the cloud. If the vertical velocity is lowered to 10 $\mathrm{m\,s^{-1}}$, the scavenging efficiency rises to 40% $\mathrm{km^{-1}}$.

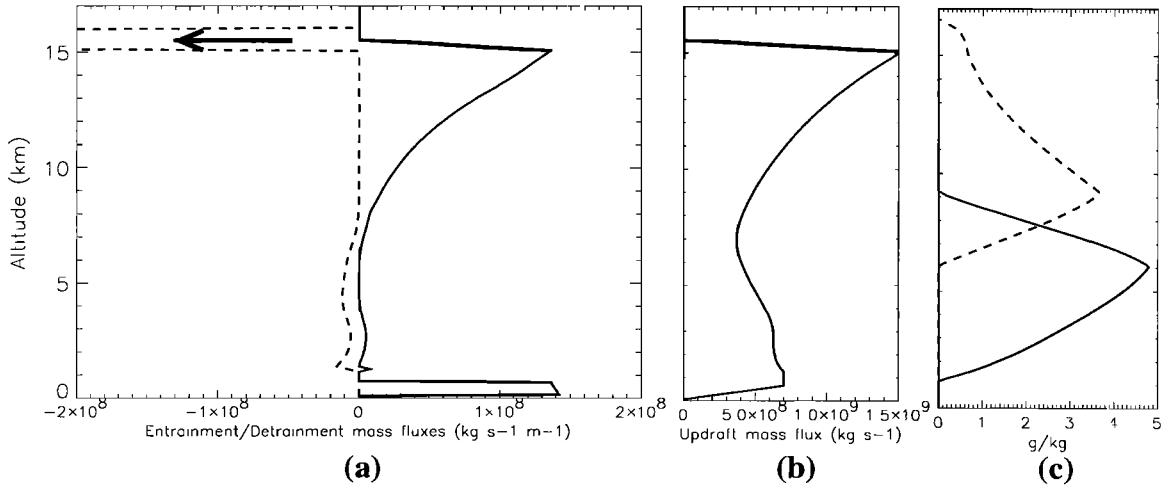

Figure 2. Simulation of a deep convective updraft over Brazil for the meteorological conditions observed during TRACE-A flight 6 on September 27, 1992. The simulation uses the 1-D entraining/detraining plume model described in section 2. (a) Vertical profiles of entrainment (solid line) and detrainment (dashed line) mass fluxes in the deep convective cloud. The arrow indicates detrainment at cloud anvil. (b) Vertical profile of the updraft convective mass flux. (c) Vertical profiles of liquid water (solid line) and ice (dashed line) mixing ratios.

2.2. Transport and Scavenging of Chemical Tracers

We have implemented in the model a tracer transport and scavenging capability fully consistent with the motion of air and water in the cloud. The efficiency of deep moist convection in scavenging a given gas or transporting it to the upper troposphere depends on the cloud condensate profile, the ratio of ice to water, the gas solubility in water and uptake on ice, as well as washout rates, updraft velocities, and turbulent entrainment at all levels. Following the mass flux formalism, the effect of the convection on the tracer mixing ratio at grid scale is given by (Bechtold et al., submitted manuscript, 2000):

$$\frac{\partial \overline{C}}{\partial t}|_{conv} = -\frac{1}{\rho A}\frac{\partial (MC)}{\partial z} - \overline{w}\frac{\partial \overline{C}}{\partial z}, \quad (7)$$

where A is the horizontal area of the grid cell (Figure 1), ρ is the air density in the cell and $\overline{w}$ is the compensational environmental subsidence. Taking into account losses from scavenging and aqueous phase reaction, the tracer mixing ratio in the convective cloud varies following:

$$\frac{\partial (MC)}{\partial z} = M_\epsilon \overline{C} - M_\delta C - \frac{MC(\alpha R c_{pr} + \beta c_{pr} + \alpha\gamma)\delta z/w}{\delta z} \quad (8)$$

where α and β (dimensionless) are the fractions of C in the liquid and solid phases respectively; R is the retention efficiency of the tracer in the condensed phase during conversion of liquid cloudwater to precipitation; and γ (s^{-1}) is the first-order rate constant for chemical loss in the liquid phase. In this paper we limit our consideration of chemical loss to liquid-phase oxidation of SO_2 by H_2O_2 and O_3. The coefficient R accounts for volatilization of tracer during riming of supercooled droplets, which is the main mechanism for precipitation of the liquid phase from mixed clouds ($248 < T < 268$ K) [*Cho and al.*, 1989]. In mixed clouds, $R \leq 1$ while in warm clouds ($T > 268$ K) $R = 1$.

The coefficient α is calculated following Henry's law equilibrium. Typical values of α are given in Table 1. Both HNO_3 and H_2O_2 are fractionated mainly in the liquid phase. Other species are mostly in the gas phase, though CH_2O and SO_2 are sufficiently water soluble to undergo significant scavenging, as discussed in the next section.

Reactive chemistry in the model is limited to aqueous phase oxidation of SO_2 in the liquid cloud, which takes place following acid-base dissociation of dissolved SO_2:

$$SO_2 \cdot H_2O \rightleftharpoons H^+ + HSO_3^-, \quad (9)$$

$$HSO_3^- \rightleftharpoons H^+ + SO_3^{2-}, \quad (10)$$

$$HSO_3^- + H_2O_2(aq) + H^+ \rightarrow SO_4^{2-} + H_2O + 2H^+ \quad (11)$$

$$SO_3^{2-} + O_3(aq) \rightarrow SO_4^{2-} + O_2. \quad (12)$$

Temperature-dependent equilibrium and rate constants for (9)-(12) are taken from *Hoffmann and Calvert* [1985] and *Hoffmann* [1986]. For the suite of other species considered here (CH_3OOH, CH_2O, H_2O_2, HNO_3), cloud chemistry is expected to have little effect on total (gas+condensed) concentrations over the 30-min maximum transport time in the cloud updraft [*Prather and Jacob*, 1997; *Jacob*, 2000]. Outside of the cloud we assume that there is no chemical tendency, that is, that the species are in steady state. Although this is clearly an oversimplification, our focus here is on the cloud scavenging processes.

Table 1. Henry's Law Constants and Gas-Liquid Partitioning in Cloud

Species	K_{298}, $M\,atm^{-1}$	$\frac{-\Delta H^0_{298}}{R}$, K	$\alpha = \frac{[X]_{aq}}{[X]_{total}}$
HNO_3[a]	3.2×10^{11}	8700	~100%
H_2O_2	8.3×10^4	7400	95%
CH_2O[b]	3.2×10^3	6800	39%
CH_3OOH	3.1×10^2	5200	4%
O_3	1.1×10^{-2}	2400	~0%
CO	9.9×10^{-4}	1300	~0%
SO_2[c]	2.4×10^3	5000	25%

The Henry's law constant K at temperature T is $K = K_{298}\, exp\{(-\Delta H^0_{298}/R)(1/T - 1/T_0)\}$ where $T_0 = 298$K. Data for K_{298} and ΔH^0_{298} are selected from measurements compiled by R. Sander (http://www.mpch-mainz.mpg.de/~sander/res/henry.html) and *Jacob* [2000]. Here $\alpha = [X]_{aq}/[X]_{total} = [1 + 1/(K\, r_c\, RT)]^{-1}$ is the dimensionless fraction of the total species concentration $[X]_{total}$ dissolved in cloud water and is given here for a cloud water mixing ratio $r_c = 2\,g\,kg^{-1}$ and T=280 K.

[a]Effective Henry's law constant for $K = [NO_3^-]/P_{HNO_3}$ at pH=5.

[b]Effective Henry's law constant $K = [H_2C(OH)_2(aq)]/P_{CH_2O}$.

[c]Effective Henry's law constant $K = [S(IV)]/P_{SO_2}$ at pH=5 accounting for $SO_2 \cdot H_2O/HSO_3^-/SO_3^{2-}$ acid-base dissociation.

While gas-liquid equilibrium can be reasonably well defined, gas-ice interactions are poorly characterized. Gas-ice partitioning is important in deep convective clouds where ice is present in a large portion of the cloud column (Figure 2). The incorporation of soluble tracers in ice depends on the mechanism for glaciation: riming or gas phase transfer of H_2O from liquid to ice. Both are important under natural conditions. In the case of HNO_3, laboratory experiments show both a high retention efficiency during riming [*Iribarne and Pyshnov*, 1990] and a rapid monolayer uptake of HNO_3 gas to ice surfaces [*Diehl et al.*, 1995; *Abbatt*, 1997; *Dominé and Thibert*, 1996]. Monolayer uptake is sufficient for total transfer of HNO_3 from the gas phase to ice at typical atmospheric ice water contents and HNO_3 concentrations [*Abbatt*, 1997]. Therefore, 100% scavenging of HNO_3 in the glaciated cloud (R=1, β=1) can be assumed for either glaciation mechanism.

In contrast, H_2O_2 scavenging by glaciated clouds appears to be less efficient. Field observations for stable wintertime cloud conditions show an average H_2O_2 retention efficiency of only 5% during riming of liquid droplets. We adopt R=0.05 in our simulation. [*Snider and Huang*, 1998]. To calculate β, we assume that uptake of H_2O_2 by growing ice crystals takes place by cocondensation [*Neftel et al.*, 1995; also P. Laj et al., manuscript in preparation, 2000] following the formulation of *Dominé et al.* [1995]:

$$X_{H_2O_2} = \frac{p_{H_2O_2}\alpha_{H_2O_2}}{p_{H_2O}\alpha_{H_2O}}\sqrt{\frac{M_{H_2O}}{M_{H_2O_2}}}. \quad (13)$$

Here $X_{H_2O_2}$ is the mole fraction of H_2O_2 in the ice, p is the partial pressure, α is the sticking coefficient on ice, and M is the molecular mass. In this manner we obtain

$$\beta_{H_2O_2} = \frac{r_i}{p_{H_2O}}\frac{\alpha_{H_2O_2}}{\alpha_{H_2O}}\sqrt{\frac{M_{H_2O}}{M_{H_2O_2}}}, \quad (14)$$

where r_i is the ice mixing ratio (moles of ice per moles of air). We adopt $\alpha_{H_2O_2}/\alpha_{H_2O}$=0.6 [*Bales and Choi*, 1996; *Haynes et al.*, 1992; also P. Laj et al., manuscript in preparation, 2000]. For T=258 K and $r_i = 3.2 \times 10^{-3}$ mol mol^{-1} (2 g kg^{-1}), we find $\beta_{H_2O_2} = 0.22$. Equilibrium between the air and ice phases yields a lower value of β than cocondensation but requires several hours to establish and therefore does not apply to ice clouds [*Conklin et al.*, 1993].

Gases other than HNO_3 and H_2O_2 are not expected to be significantly scavenged by the ice. The retention efficiency of SO_2 during riming is about 2% [*Voisin et al.*, 2000]. SO_2 is more likely incorporated into ice by trapping in the quasi-liquid layer on ice surfaces growing by deposition [*Mitra et al.*, 1990]. However, at very low temperatures encountered in deep convective clouds, a quasi-liquid layer is unlikely to remain, and uptake of SO_2 decreases with temperature as the fraction of liquid decreases [*Conklin and Bales*, 1993]. CH_2O in rimed ice is released quickly to the atmosphere [*Hutterli et al.*, 1999]. We assume R=0.02 and β=0. for SO_2, CH_2O , and CH_3OOH.

3. Cloud Simulation Results

3.1. Dynamical Environment

We applied the 1-D convective plume model to a severe continental convective event observed during flight 6 of the 1992 TRACE-A aircraft experiment over Brazil [*Fishman et al.*, 1996]. That flight, conducted on September 27, was devoted to sampling the outflow from a deep convective system that had developed over a region strongly affected by biomass burning pollution. Observations of a large number of chemical species including CO, HNO_3, H_2O_2, CH_3OOH , and CH_2O (but not SO_2) were made aboard the aircraft and can be used to constrain and evaluate the model. Detailed meteorological and chemical analyses for this particular convective event have been reported previously [*Thompson et al.*, 1997; *Pickering et al.*, 1996]. Convective activity began in southern Brazil, associated with a cold frontal system pushing northeastward from the midlatitudes of the Southern Hemisphere. By September 25 a strong zone of low-level convergence persisted and advanced rapidly northward. Large mesoscale convective systems developed on September 26 along a west-east line of convergence centered on about 8°S and later along a north-south line located between 8° and 15°S, centered on about 50°W. The north-south oriented line developed by 2130 UT, and peak development was at about 0130 UT on September 27. Cloud top temperatures in this system were less than 205 K, corresponding to cloud top heights of at least 15 km. It is this system that we simulate with the 1-D entraining/detraining plume model. The model domain covers a 100×100 km region centered around 11.5°S and 47.5°W.

The aircraft conducted a series of ascents, descents and constant-altitude segments in the column extending up to 12 km (ceiling of the aircraft) to capture outflow from the convective system. The flight covered a region from 8° to 16°S and 44° to 49°W. *Pickering et al.* [1996] defined cloud outflow regions using a combination of measured CO and satellite imagery. Enhanced upper tropospheric CO mixing ratios measured in areas around cold cloud tops seen on IR satellite imagery were considered to be indicative of cloud outflow. Outflow was encountered several times, in particular on flight legs at 9.5 and 11.3 km altitude.

We performed a 1-D simulation extending from September 26 at 1800 UTC to September 27 at 1200 UTC. Figure 2 shows simulated profiles of the convective air mass fluxes and condensate mixing ratios on September 27 at 0000 UTC during the maximum intensity of the convective system [*Pickering et al.*, 1996]. At the peak of convection intensity, the CAPE value from the ECMWF analysis is 2500 J kg^{-1}. The correspond-

ing simulated maximum mixing ratio of condensate is 4.8 $g\,kg^{-1}$. The model produces a maximum vertical velocity of 25 $m\,s^{-1}$ with overshoot at 16 km. Temperature in the convective cloud decreases from 290 K at cloud base (1 km) to 190 K at cloud top (16 km).

The convective upward mass flux increases from the surface to 1 km (altitude of the cloud base). It then decreases up to 7 km and increases again up to cloud top at 15-16 km. The updraft entrains air from the environment at most levels, particularly at 0-1 km (below cloud base) and from 7 to 15 km, where entrainment serves to rapidly increase the upward flux. The entrainement above 7 km is driven by glaciation of the cloud, increasing its buoyancy; as pointed out above, glaciation also suppresses scavenging of the gases of interest except HNO_3. Cloud detrainment is mostly at 1-7 km and in the cloud anvil at 15-16 km. The cloud top in the model rises gradually as the cloud matures. As a consequence, detrainment at cloud top occurs at different rising levels during the cloud history, gradually modifying the free troposphere with boundary layer air. This modified free tropospheric air can then be reentrained in the cloud as the convection deepens, producing a convective ladder effect.

3.2. Convective Transport of Soluble Gases

We simulate the transport and scavenging within the convective model plume of HNO_3, H_2O_2, CH_2O, CH_3OOH, SO_2 and CO. Because of its low solubility, CO serves as an inert tracer. The initial mixing ratio profiles for preconvective conditions are specified from measurements made during TRACE-A flight 6 in the background atmosphere, that is, excluding convective outflow. The initial mixing ratio profile for SO_2 is specified from measurements made during the Atmospheric Boundary Layer Experiment (ABLE) campaigns over the Amazonian basin during the dry and wet seasons [*Andreae and Andreae*, 1988; *Andreae et al.*, 1990a]. Typical values were 25 pptv in the boundary layer and 15 pptv in the free troposphere. Convective outflow in the TRACE-A flight 6 data above 7 km is diagnosed by CO mixing ratio > 170 ppbv. Postconvective model profiles sampled on the grid scale (i.e., in the environmental air outside the updraft) can then be compared to the convective outflow observations for different species as a test of the model.

Comparisons of average mixing ratios at 7-12 km altitude for the preconvective (background) and postconvective (convective outflow) atmospheres are shown in Table 2 for both model and observations. The agreement between observed and simulated background mixing ratios simply follows from the model initialization. We define the convective enhancement factor (CEF) at 7-12 km altitude as the ratio of gases mixing ratios in the convective outflow (i.e., after convective cloud venting and scavenging of gases) relative to the background (i.e., without deep convection effects). The CEF for a given species depends on its vertical mixing ratio profile in the background atmosphere and on its solubility (i.e., scavenging efficiency). As shown in Table 2, the model simulates well the observed gradation of CEF between species of different solubility. The CEF is highest for CH_3OOH which is only sparsely soluble and has a strong gradient of decreasing mixing ratio with altitude in the background atmosphere. The CEF is lowest (below unity) for HNO_3 , which is quantitatively scavenged

Table 2. Observed and Simulated Mixing Ratios at 7-12 km Altitude for Preconvective and Postconvective Conditions, and Convective Enhancement Factors (CEF)

	Observed Background	Observed Convective Outflow	Observed CEF	Simulated Background	Simulated Convective Outflow	Simulated CEF
CO	97 ± 22 (n=1282)	234 ± 36 (n=918)	2.4	101	192	1.9
CH_3OOH	36 ± 209 (n=27)	390 ± 186 (n=15)	11	40	383	9.5
CH_2O	153 ± 27 (n=30)	444 ± 229 (n=11)	2.9	163	513	3.1
H_2O_2	340 ± 274 (n=27)	651 ± 533 (n=15)	1.9	337	410	1.2
HNO_3	60 ± 26 (n=10)	50 ± 32 (n=5)	0.8	60	24	0.4
SO_2				15	7-14.3	0.5 - 0.9

Volume mixing ratios are in units of parts per billion by volume for CO and parts per trillion per volume for the other species. Data are for the TRACE-A flight 6 on September 22, 1992 over eastern Brazil. Convective outflow at 7-12 km altitude is diagnosed in the observations by CO mixing ratios in excess of 170 ppbv, and in the model by sampling the grid-scale environment for postconvective conditions after 6 hours of simulation. The background preconvective atmosphere in the model is specified from observations, hence the similarity between observed and simulated background. The convective enhancement factor (CEF) is the ratio of mixing ratio in the convective outflow and the background. The range of SO_2 convective enhancement factors from the four scenarios (pH=4-6 and O_3=20 ppbv; pH=5 and O_3=20-50 ppbv) is presented.

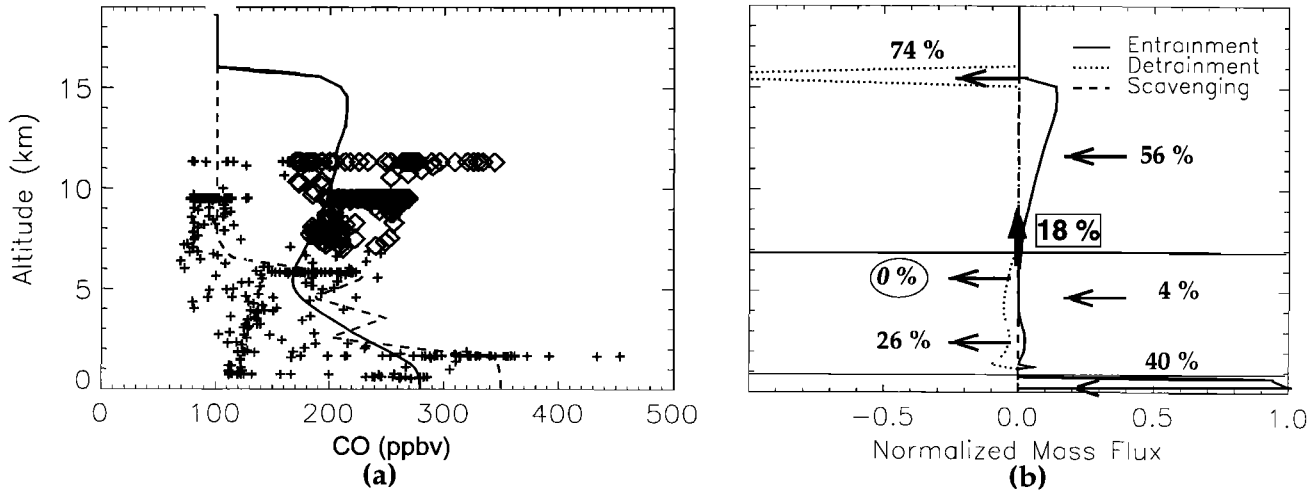

Figure 3. (a) Vertical profiles of CO mixing ratio for TRACE-A flight 6. Model vertical profiles are shown for the preconvective background atmosphere (dashed line) and for the postconvective atmosphere after 6 hours of simulation (solid line). Observed CO mixing ratios are shown as symbols for the background atmosphere (pluses) and for convective outflow above 7 km (diamonds). Convective outflow in the observations above 7 km is diagnosed by CO > 170 pptv. (b) Budget of CO in the convective model cloud. The lines show the vertical profiles of entrainment (solid), detrainment (dotted) and scavenging (dashed, percentage in oval frame) mass fluxes in the convective cloud for CO. Profiles are normalized to the entrainment mass flux at cloud base. Percentage contributions of entrainment, detrainment, and scavenging to the CO budget in the convective column are given for three vertical regions: below cloud base, between 1 and 7 km, and from 7 km to cloud top. The percentages are computed relative to the total entrained mass flux integrated over the depth of the convective column. The percentage in the rectangular frame gives the upward tracer flux at 7 km altitude, where the cloud glaciates (Figure 2), for comparison to the entrainment flux in the glaciated cloud at higher altitudes.

by both liquid and ice precipitation; HNO_3 is depleted in convective outflow. In the discussion that follows, we examine in more detail the budgets of individual species in the convective cloud.

3.2.1. CO. Vertical profiles and convective model budgets for CO are shown in Figure 3. The background mixing ratio profile features high boundary layer mixing ratio (350 ppbv) due to the regional-scale biomass burning influence. The background mixing ratio in the upper troposphere at 7-12 km altitude is about 100 ppbv (Table 2). Convection causes significant vertical redistribution of CO. The postconvective vertical profile at grid scale (Figure 3) shows a dramatic increase of CO mixing ratio in the upper troposphere, with values above 200 ppbv both in the model and in observations. The CEF at 7-12 km altitude is 2.4 in the observations and 1.9 in the model (Table 2).

The budget calculation in Figure 3 reveals that more than half (56%) of the CO entrained in the cloud is drawn from the glaciated region in the upper part of the cloud (from 7 to 15 km), 40% of CO is entrained below the cloud base, and 4% is entrained between the cloud base and 7 km. Most of the 44% of the CO entrained in the lower part of the cloud is detrained near the cloud base (26%); 18% is transported upward to the upper troposphere above 7 km while 74% of the CO entrained in the cloud is detrained in the cloud anvil, most of that CO originates in the upper troposphere (7-15 km). In the model this upper tropospheric reservoir has been previously enriched at the earlier, less deep, stage of the convective cloud development. Reentrainment of that air in the cloud represents the convective ladder effect.

The importance of high-altitude entrainment in our simulation reflects the buoyancy associated with the glaciation of the cloud. It is consistent with previous studies suggesting that a large fraction of the air detrained at cloud anvil height is drawn from the midtroposphere [*Dickerson et al.*, 1987; *Wang and Chang*, 1993; *Scala et al.*, 1990]. A simulation by *Scala et al.* [1990] of a deep convective event over Amazonia found that more than half of the air transported to the anvil height originated above 6 km altitude, not from the planetary boundary layer. It appears that direct pumping from the boundary layer to the upper troposphere accounts for only a small fraction of the air in convective outflows, contrary to the assumption made in simple nonentraining convective plume models [*Prather and Jacob*, 1997; *Cohan et al.*, 1999]

3.2.2. CH_3OOH. The simulated cloud outflow vertical profile of CH_3OOH in Figure 4 exhibits a strong increase of mixing ratio above 7 km, consistent with observations. Background mixing ratio in the upper troposphere is 30-40 pptv. Both modeled and observed mixing ratios reach in excess of 300 pptv after the con-

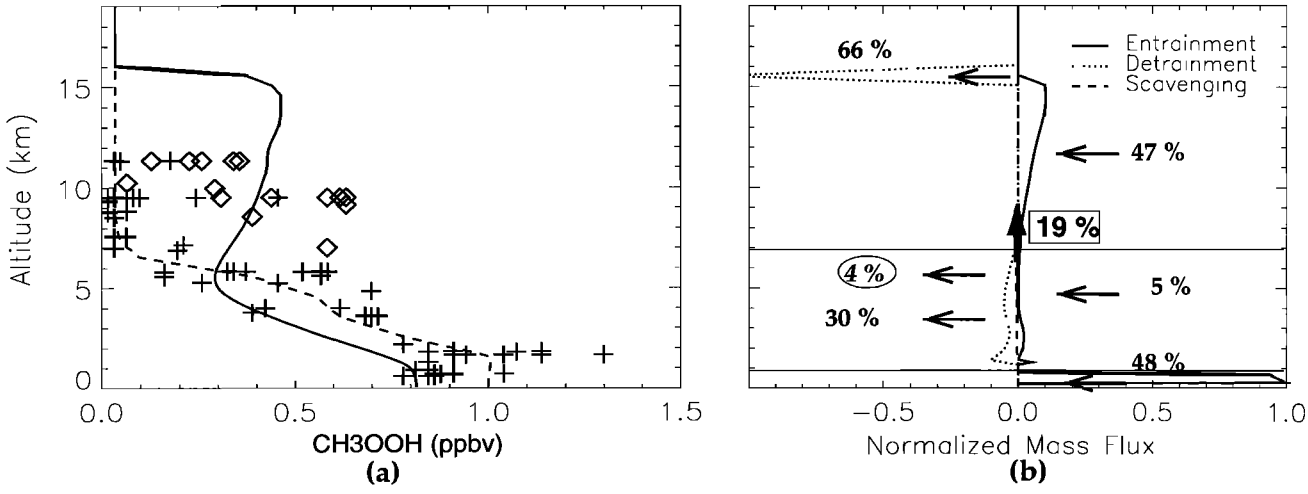

Figure 4. Same as Figure 3, but for CH_3OOH.

vection event (Table 2). The observed CEF of 11 is comparable although higher than the CEF of 6 previously observed in deep marine convection over the South Pacific [*Cohan et al.*, 1999]. The CEF is much larger than for CO because of the stronger contrast in background mixing ratios between the lower and upper troposphere.

We see from Figure 4 that 66% of CH_3OOH entrained in the cloud is detrained at cloud anvil height. As for CO, most of this 66% originates from high-altitude entrainment in the glaciated cloud (47%). The remaining 19% originates mainly from entrainment below cloud base. A negligible fraction of CH_3OOH entering the updraft (4%) is scavenged. As in the case of CO, the entrained CH_3OOH at 7-15 km is heavily influenced by previous convective enrichment which took place in an earlier stage of the cloud.

3.2.3. CH_2O. The simulated cloud outflow vertical profile for CH_2O (Figure 5) exhibits an increase of upper tropospheric mixing ratios relative to the background profile from 163 pptv to 513 pptv. The model CEF is 3.1, comparable to the value of 2.9 found in the observations (Table 2). High-altitude entrainment is less than for CH_3OOH as the 7-15 km entraining layer is relatively less enriched in CH_2O than in CH_3OOH. The main reason is scavenging of CH_2O in the warm cloud removing 23% of the CH_2O entrained in the updraft; the Henry's law solubility of CH_2O (Table 1) puts it at the threshold for efficient scavenging. Detrainment below cloud anvil height and scavenging by liquid precipitation account for comparable losses of CH_2O (23% and 26% respectively). As seen in Figure 5, 51% of the CH_2O entering the cloud is released at the cloud anvil height and can eventually participate in upper tropospheric chemistry. Our results indicate that scavenging of CH_2O in deep convection cannot be neglected, contrary to the common assumption [*Müller and Brasseur*, 1999].

3.2.4. H_2O_2. The initial background mixing ratio of H_2O_2 is about 7 ppbv below 2 km and less than 500 pptv in the upper troposphere (Figure 6), reflecting

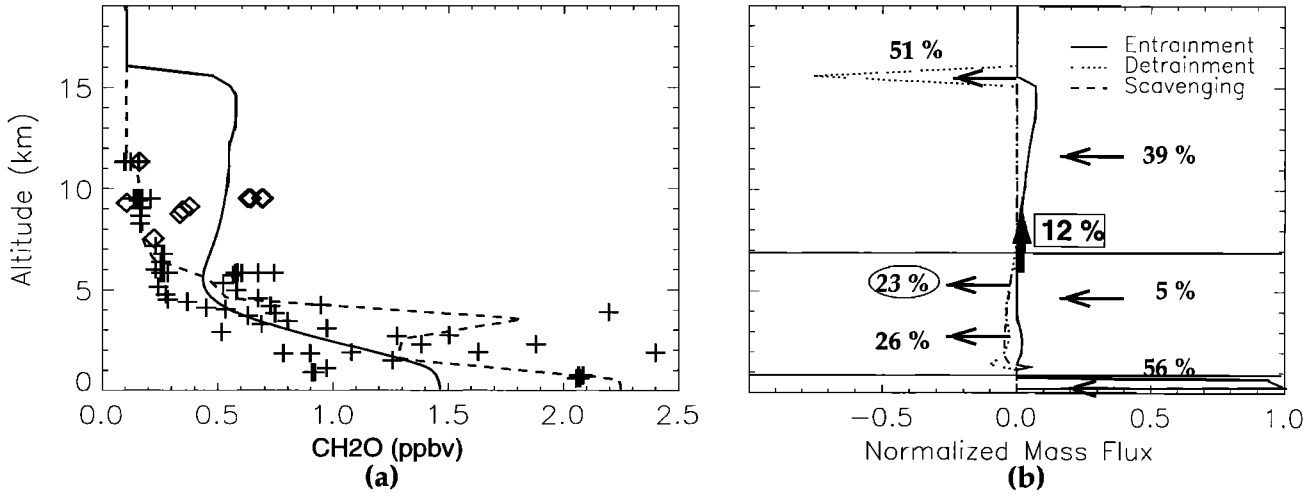

Figure 5. Same as Figure 3, but for CH_2O.

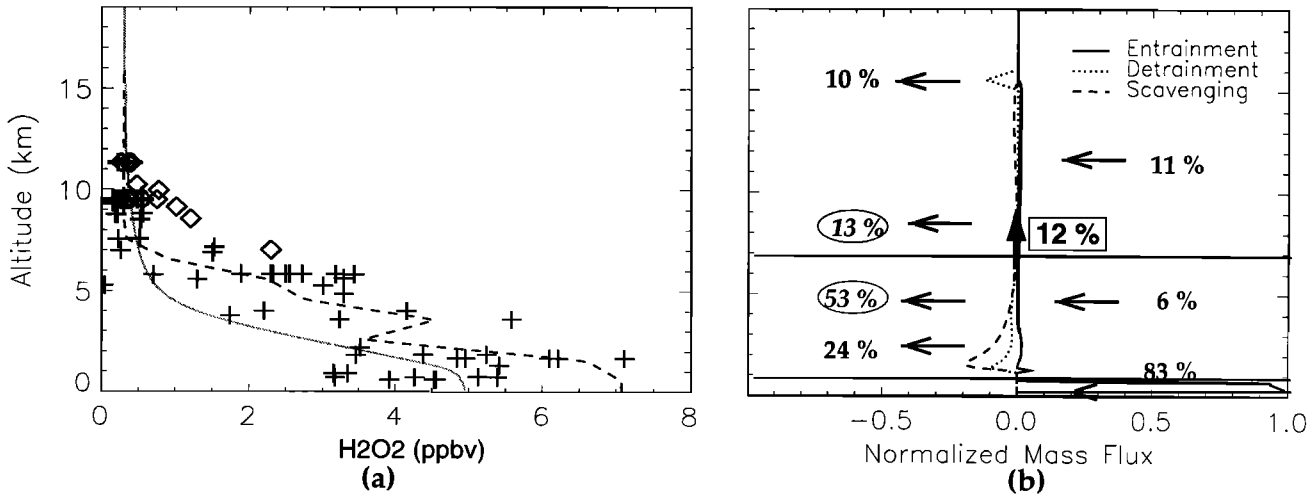

Figure 6. Same as Figure 3, but for H_2O_2.

the vertical gradient of water vapor, which is the main chemical precursor for H_2O_2 [*Jacob et al.*, 1996]. In our case, SO_2 mixing ratios are sufficiently low not to affect the H_2O_2 budget. The high Henry's law constant for H_2O_2 (Table 1) implies efficient scavenging in the warm cloud, but scavenging is suppressed in the mixed cloud due to volatilization of H_2O_2 from rimed ice. As a result we find in the model that deep convection increases H_2O_2 mixing ratios in the upper troposphere, consistent with observations (Table 2). The model CEF (1.2) is somewhat lower than the observed CEF (1.9). The observations were made in early morning to mid-morning [*Pickering et al.*, 1996], so that chemical production in the outflow probably cannot account for the discrepancy. A comparable CEF of 1.7 for H_2O_2 was previously observed in deep marine convection over the tropical Pacific [*Cohan et al.*, 1999].

Model results indicate that 10% of H_2O_2 entering the cloud is detrained at cloud anvil height (Figure 6). This H_2O_2 originates mainly from H_2O_2 entrained from the 7-15 km region. We find that 53% of H_2O_2 entering the convective cloud below 7 km is scavenged by liquid precipitation, and most of the remainder is detrained at low altitude; only 12% is pumped above 7 km (Figure 6). Nevertheless, this small fraction accumulating over the cloud history is responsible for the enhancement of H_2O_2 in the convective outflow. In a sensitivity simulation we found that ignoring the volatilization of H_2O_2 from rimed ice in the mixed cloud results in a depletion of H_2O_2 in the convective outflow (CEF=0.5) due to efficient scavenging in the mixed cloud. Such a depletion would be contrary to observations [*Pickering et al.*, 1996; *Jaeglé et al.*, 1997; *Cohan et al.*, 1999] There seems therefore to be good evidence that cloud glaciation suppresses H_2O_2 scavenging.

3.2.5. HNO_3. Nitric acid is ~100% fractionated into the condensed phase in both warm and glaciated clouds (section 2.2). Its scavenging thus follows that of condensed water and is highly efficient. Mixing ratios in the convective outflow are depleted relative to

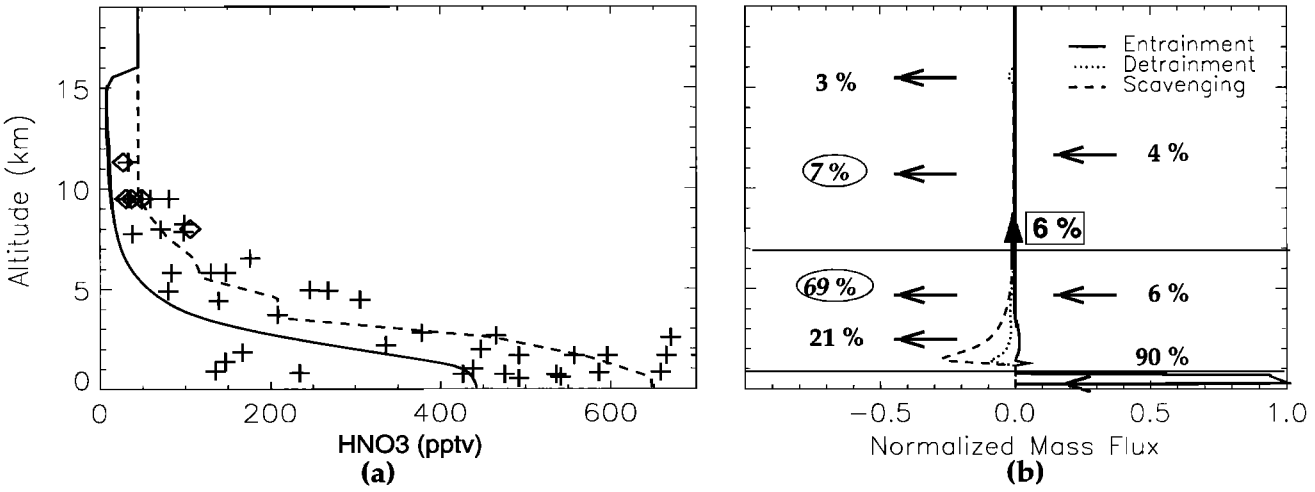

Figure 7. Same as Figure 3, but for HNO_3.

background, both in the model and in the observations (Figure 7 and Table 2). The CEF in the model (0.4) is somewhat lower than observed (0.8), but is consistent with the value of 0.3 previously observed for deep marine convection over the tropical Pacific [*Cohan et al.*, 1999]. As seen in Figure 7, most of HNO_3 enters the updraft below cloud base (90%). As 69% of HNO_3 is scavenged by liquid precipitation below 7 km, only 6% of HNO_3 is transported upward. Of the 10% of HNO_3 entering the cloud above 7 km via upward flux (6%) or lateral entrainment (4%), a major part is scavenged by snow (7%). Only 3% of HNO_3 is detrained at cloud anvil height.

3.2.6. SO_2. There were no measurements of SO_2 during the TRACE-A campaign. We specify the background preconvective profile from measurements made during the ABLE 2A and ABLE 2B aircraft experiments over Amazonia. Scavenging of SO_2 in the model cloud takes place by dissolution and aqueous phase oxidation by H_2O_2 and O_3. The calculation uses H_2O_2 obtained from the model (Figure 6). Mixing ratios of O_3 are specified either at 50 ppbv, corresponding to the polluted conditions of TRACE-A flight 6 [*Pickering et al.*, 1996], or at 20 ppbv, which is a more typical value for the tropics.

As seen from reactions (9)-(12), the rate of oxidation of SO_2 by H_2O_2 is pH-independent over the pH range of atmospheric interest; by contrast, the rate of oxidation by O_3 varies as $[H^+]^{-2}$. A sensitivity analysis is performed for different values of pH (4-6). This range of pH values is typical of precipitation over the Amazonian basin [*Andreae et al.*, 1990b]. The pH is assumed uniform across the cloud droplet population. At pH of 5 and lower, aqueous phase reaction of SO_2 by H_2O_2 is dominant; at pH=6, oxidation by O_3 prevails. The model budget in Figure 8 shows that at pH=5 (pH=4), 54% (59%) of SO_2 entering the cloud is detrained at the cloud anvil height. This proportion is lowered to 28% for pH=6 and 20 ppbv O_3. At pH=5, we find that 29% of SO_2 is scavenged from the warm cloud, most of it by aqueous phase reaction with H_2O_2. At pH=6, this scavenging increases to 50% (O_3=20 ppbv) and 63% (O_3=50ppbv).

Figure 8 shows the simulated vertical profiles of SO_2 in the postconvective atmosphere for the different values of pH and O_3 mixing ratio. Under all conditions, SO_2 is depressed in the convective outflow relative to the background atmosphere (Table 2). This result is consistent with observations in outflow of deep marine convection over the tropical Pacific [*Thornton et al.*, 1997; *Cohan et al*, 1999]

3.2.7. Sensitivity to the condensate conversion rate, c_{pr}. The first-order rate constant c_{pr} for conversion of liquid and ice cloud condensate to precipitation is a key parameter in our simulation. The sensitivity of scavenging efficiencies and CEF to various values of c_{pr} is shown in Table 3. When c_{pr} is large, hydrometeors are produced rapidly, and scavenging of chemical species is efficient. However, the response of the model to c_{pr} involves more than just scavenging. Changing c_{pr} also modifies the convection dynamics; removal of the precipitated water (and the consequent strong drag force) tends to counteract the buoyancy force, preventing further development of the cloud. The comparison of simulated and observed CEF (Table 2) provides a way to constrain the value for

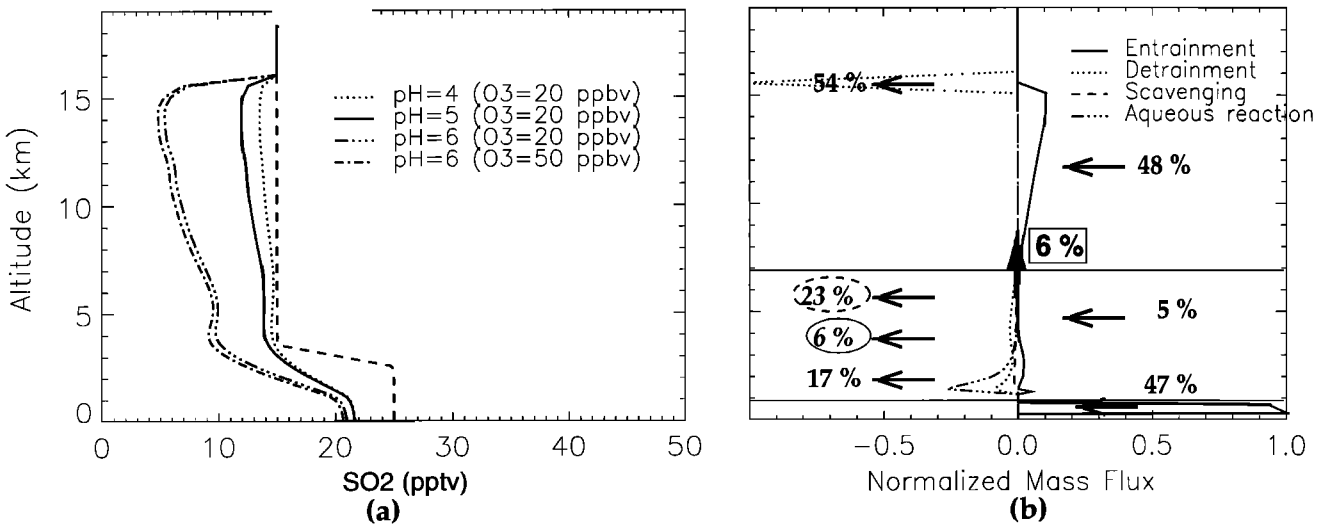

Figure 8. Same as Figure 3, but for SO_2. Only model results are shown as no observations were made in TRACE-A. (a) Postconvective vertical profiles are shown for three different assumed values of cloud water pH and at pH=6, for two different mixing ratios of ozone. (b) The convective column budget is shown for the case with cloud water pH=5 and ozone mixing ratio 20 ppbv; the dashed oval gives the contributions to the budget from loss by aqueous phase oxidation in the cloud.

Table 3. Scavenging Efficiency (SE) and Convective Enhancement Factor (CEF) of Gases in Deep Convection

c_{pr}, s^{-1}	0.001		0.005		0.01		0.02	
	SE, %	CEF	SE, %	CEF	SE, %	CEF	SE, %	CEF
CH_3OOH	1	12	5	9.5	6	8.5	7	8
CH_2O	2	5	23	3	36	2.3	47	1.7
H_2O_2	25	4.2	66	1.2	84	0.4	90	0.3
HNO_3	32	1.6	77	0.4	87	0.2	93	0.1
SO_2	13	0.8	28	0.9	29	0.9	27	0.9

The table shows for each gas the convective enhancement factor at 7-12 km altitude (CEF) and the scavenging efficiency (percent) defined as the mass percentage of gas entering the convective cloud that is scavenged by convective precipitation. Values are shown as a function of the rate constant c_{pr} for conversion of cloudwater to precipitation. The scavenging efficiency for SO_2 is given for cloud water pH=5 and O_3=20 ppbv and includes losses by aqueous phase oxidation plus liquid precipitation of dissolved SO_2.

c_{pr}. For c_{pr} equal to 0.01 s^{-1}, H_2O_2 is depleted in the outflow (simulated CEF<1), in disagreement with the observations (observed CEF=1.5). For c_{pr}=0.001 s^{-1}, HNO_3 mixing ratios are found to increase in the upper troposphere (simulated CEF=1.6), whereas observations indicate a decrease (observed CEF=0.8). There is therefore some support for our adoption of c_{pr}=0.005 s^{-1} in the standard model.

We see from Table 3 that the solubility of CH_2O places it at the threshold for efficient scavenging, with a scavenging efficiency of 23% in the standard case (c_{pr}=0.005 s^{-1}) but varying from 2% to 47% over the range of c_{pr}=0.001-0.02 s^{-1}. Less soluble species like CH_3OOH are less sensitive to the choice of c_{pr} and are poorly scavenged in any case. The scavenging efficiency and CEF for SO_2 is only moderately sensitive to c_{pr} because of compensating effects. When c_{pr} is large, scavenging of dissolved SO_2 by precipitation is more efficient. However, H_2O_2 is also efficiently scavenged, slowing down the rate of SO_2 oxidation.

4. Conclusion

A one-dimensional entraining/detraining convective plume model driven by ECMWF meteorological fields has been used to simulate a tropical continental deep convective system observed during the TRACE-A aircraft campaign over eastern Brazil. Convective transport and scavenging of gases with different Henry's law solubilities were examined including CO (inert tracer), CH_3OOH, CH_2O, H_2O_2, HNO_3 , and SO_2. Glaciation of the cloud in the midtroposphere has important implications for scavenging. There is good experimental evidence that HNO_3 remains in the ice phase during and after glaciation, while other gases are expelled to the gas phase.

Observed (simulated) convective enhancement factors (CEF) at 7-12 km altitude, representing the ratios of postconvective to preconvective mixing ratios, are 2.4 (1.9) for CO, 11 (9.5) for CH_3OOH, 2.9 (3.1) for CH_2O, 1.9 (1.2) for H_2O_2, and 0.8 (0.4) for HNO_3. The large CEF for CH_3OOH reflects its low solubility and its boundary layer enrichment relative to the upper troposphere. The observed CEF values are consistent with a rate constant c_{pr}=0.005 s^{-1} for conversion of cloud condensate to precipitation.

The Henry's law constant for CH_2O puts it at the threshold for efficient scavenging; in our standard simulation, 23% of CH_2O entering the convective plume is scavenged.

Both HNO_3 and H_2O_2 are efficiently scavenged in the warm cloud, but only HNO_3 is efficiently scavenged in both the mixed and glaciated cloud. The low retention efficiency of H_2O_2 in rimed ice shuts off H_2O_2 scavenging in the mixed cloud. This can explain the consistent observation, in TRACE-A and elsewhere, that H_2O_2 is enhanced in deep convective outflows while HNO_3 is depleted.

A substantial fraction of SO_2 entrained in the convective cloud is scavenged by aqueous reaction with H_2O_2 and O_3 (23% at pH=5, 50% at pH=6). As a consequence, mixing ratios of SO_2 are depleted in the convective outflow. The latter result depends on the gradient in SO_2 mixing ratios between the boundary layer and the free troposphere in the preconvective atmosphere. In our case this gradient is relatively weak.

Model results indicate little direct transfer of air from the boundary layer to the cloud anvil in the convective plume, because of low-level detrainment in the warm cloud and high-level entrainment in the glaciated cloud. The importance of high-level entrainment contradicts simple model representations of deep convection as a nonentraining pipe transferring air from the boundary layer to the upper troposphere. However, the air entrained at high levels has a strong boundary layer influence, reflecting its detrainment from the plume in an earlier, less deep stage of the cloud. The resulting convective ladder effect can transfer air from the boundary

layer to the upper troposphere with relatively little dilution, in a manner that may in the end show some similarity to the nonentraining pipe model.

Our one-dimensional entraining/detraining plume model is obviously a gross simplification of the actual transport and scavenging that occur in real convective clouds. However, the favorable comparison to convective outflow observations presented in this study suggests that the model may provide a powerful approach for parameterizing deep convection in three-dimensional global and regional chemical transport models.

Acknowledgments. This work has been supported by NASA/ SASS, PNCA/CNRS/INSU, and the Société de Secours des Amis des Sciences. We wish to thank Paolo Laj from Laboratoire de Météorologie Physique and Jeff Snider from University of Wyoming for useful discussions.

References

Abbatt, J.P.D., Interaction of HNO_3 with water-ice surfaces at temperatures of the free troposphere, *Geophys. Res. Lett., 24*, 1479–1482, 1997.

Andreae, M.O., and T.W Andreae, The cycle of biogenic sulfur compounds over the Amazonian Basin, 1. Dry season, *J. Geophys. Res., 93*, 1487–1497, 1988.

Andreae, M.O, H. Berresheim, H. Bingemer, D.J. Jacob, B.L. Lewis, S.-M. Li, and R.W. Talbot, The atmospheric sulfur cycle over the Amazonian Basin, 2. Wet season, *J. Geophys. Res., 95*, 16,813–16,824, 1990a.

Andreae, M.O., R.W. Talbot, H. Berresheim, and K.M. Beecher, Precipitation chemistry in central Amazonia, *J. Geophys. Res., 95*, 16987–16999, 1990b.

Andronache, C., L.J. Donner, C.J. Seman, V. Ramaswamy, and R.S. Hemler, Atmospheric sulfur and deep convective clouds in tropical Pacific: A model study, *J. Geophys. Res., 104*, 4005-4024, 1999.

Bales, R.C. and J. Choi, Conceptual framework for interpretation of exchange processes, in *Chemical Exchange Between the Atmosphere and Polar Snow, NATO ASI, Series, vol. I 43*, pp. 319-338, Springer-Verlag, Berlin Heidelberg, 1996.

Barth, M.C., Numerical modeling of sulfur and nitrogen chemistry in a narrow cold-frontal rainband: The impact of meteorological and chemical parameters, *J. Appl. Meteorol., 33*, 855-868, 1994.

Bechtold, P., J. L. Redelsperger, I. Beau, M. Blackburn, S. Brinkop, J. Y. Grandpeix, A. Grant, D. Gregory, F. Guichard, C. Hoff, and E. Ioannidou, A GCSS model intercomparison for a tropical squall line observed during TOGA-COARE, II, Intercomparison of SCMs and with CRM, *Q. J. R. Meteorol. Soc.*, in press, 2000.

Chatfield, R.B. and P.J. Crutzen, Sulfur dioxide in remote oceanic air: cloud transport of reactive precursors, *J. Geophys. Res., 89*, 7111–7132, 1984.

Cho, H.R., N. Niewiadomski, and J.V. Iribarne, A model of the effect of cumulus clouds on the redistribution and transformation of pollutants, *J. Geophys. Res., 94*, 12,895–12,910, 1989.

Cohan, D.S., M.G. Schultz, D.J. Jacob, B.G. Heikes, and D.R. Blake, Convective injection and photochemical decay of peroxides in the tropical upper troposphere: Methyl iodide as a tracer of marine convection, *J. Geophys. Res., 104*, 5717–5724, 1999.

Conklin, M.H., and R.C. Bales, SO_2 uptake on ice spheres: Liquid nature of the ice-air interface, *J. Geophys. Res., 98*, 16,851–16,855, 1993.

Conklin, M.H., A. Sigg, A. Neftel, and R.C. Bales, Atmosphere-snow transfer function for H_2O_2: microphysical considerations, *J. Geophys. Res., 98*, 18,367–18,376, 1993

Cotton, W.R., G.D. Alexander, R. Hertenstein, R.L. Walko, R.L. McAnelly, and M. Nicholls, Cloud venting-A review and some new global annual estimates, *Earth Sci. Rev., 39*, 169-206, 1995.

Dickerson, R.R. et al., Thunderstorms: An important mechanism in the transport of air pollutants, *Science, 235*, 460–464, 1987.

Diehl, K., S.K. Mitra, and H.R. Pruppacher, A laboratory study of the uptake of HNO_3 and HCl vapor by snow crystals and ice spheres at temperatures between 0 and -40°C, *Atmos. Environ., 29*, 975–981, 1995.

Dominé, F., and E. Thibert, Mechanism of incorporation of trace gases in ice grown from the gas phase, *Geophys. Res. Lett., 23*, 3627–3630, 1996.

Dominé, F., E. Thibert, E. Silvente, M. Legrand, and J.-L. Jaffrezo, Determining past atmospheric HCL mixing ratios from ice core analyses, *J. Atmos. Chem., 21*, 165–186, 1995.

Fishman, J., J. M. Hoell Jr, R.D. Bendura, R.J. McNeal, and V.W.J.H Kirchhoff, The NASA GTE TRACE-A Experiment (September-October 1992), *J. Geophys. Res., 101*, 23,865–23,879, 1996.

Flossmann, A.I., and W. Wobrock, Venting of gases by convective clouds, *J. Geophys. Res., 101*, 18,639–18,649, 1996.

Fritsch, J.M., and C.F. Chappell, Numerical prediction of convectively driven mesoscale pressure system, Part I: Convective parameterization, *J. Atmos. Sci., 37*, 1722–1733, 1980.

Giorgi, F., and W.L. Chameides, Rainout lifetimes of highly soluble aerosols and gases as inferred from simulations with a general circulation model, *J. Geophys. Res., , 91*, 14367–14376, 1986.

Haynes, D.R., N.J. Tro, and S.M. George, Condensation and evaporation of H_2O on ice surfaces, *J. Phys. Chem., 96*, 8502–8509, 1992.

Hoffmann, M.R., On the kinetics and mechanism of oxidation of aquated sulfur dioxide by ozone, *Atmos. Environ., 20*, 1145–1154, 1986.

Hoffmann, M.R., and J.G. Calvert, Chemical transformation modules for Eulerian acid deposition models, vol. 2, The aqueous-phase chemistry, *Rep. EPA/600/3-85/017*, U.S. Environ. Protect. Agency, Research Triangle Park, N.C., 1985.

Hutterli, M.A., R. Rothlisberger, and R.C. Bales, Atmosphere-to-snow-to-firn transfer studies of HCHO at Summit, Greenland, *Geophys. Res. Lett., 26*, 1691-1694, 1999.

Iribarne, J.V. and T. Pyshnov, The effect of freezing on the composition of supercooled droplets-I. Retention of HCl, HNO_3, NH_3 and H_2O_2, *Atm. Env., 24A*, 383–387, 1990.

Jacob, D.J., Heterogeneous chemistry and tropospheric ozone *Atmos. Environ., 34*, 2131–2159, 2000.

Jacob, D.J. et al., Origin of ozone and NO_x in the tropical troposphere: A photochemical analysis of aircraft observations over the South Atlantic basin, *J. Geophys. Res., 101*, 24235–24250, 1996.

Jaeglé, L., et al., Observed OH and HO_2 in the upper troposphere suggest a major source from convective injection of peroxides, *Geophys. Res. Lett., 24*, 3181–3184, 1997.

Jaeglé, L., D.J Jacob, W.H. Brune, A.J. Weinheimer, B.A. Ridley, T.L. Campos, and C.W. Sachse, Sources of HO_x and production of ozone in the upper troposphere over the United States, *Geophys. Res. Lett., 25*, 1709–1712, 1998.

Kain, J.S., and J.M. Fritsch, A one-dimensional entrain-

ing/detraining plume model and its application in convective parametrization, *J. Atmos. Sci., 47*, 2784–2802, 1990.

Lafore, J.P., et al., The Meso-NH Atmospheric simulation system, I. Adiabatic formulation and control simulations, *Ann. Geophys., 16,* 90-109, 1998.

Lamarque, J.-F., G.P. Brasseur, P.G. Hess, and J.-F. Mller, Three-dimensional study of the relative contributions of the different nitrogen sources in the troposphere, *J. Geophys. Res., 101*, 22,955–22,968, 1996.

McKeen, S.A., T. Gierczak, J.B. Burkholder, P.O. Wennberg, T.F. Hanisco, E.R. Keim, R.-S. Gao, S.C. Liu, A.R. Ravishankara, and D.W. Fahey, The photochemistry of acetone in the upper troposphere: A source of odd-hydrogen radicals, *Geophys. Res. Lett., 24,* 3177-3180, 1997.

Mitra, S.K., S. Barth, and H.R. Pruppacher, A laboratory study on the scavenging of SO_2 by snow crystals, *Atmos. Environ., 24A*, 2307–2312, 1990.

Müller, J.-F., and G. Brasseur, Source of upper tropospheric HO_x : A three-dimensional study, *J. Geophys. Res., 104*, 1705–1715, 1999.

Neftel, A., R.C. Bales, and D.J. Jacob, H_2O_2 and HCHO in polar snow and their relation to atmospheric chemistry, in *Ice Core Studies of Global Biogeochemical Cycles, NATO ASI Series, vol I 30,* edited by R.J. Delmas, pp. 249–264, Springer-Verlag, Berlin Heidelberg, 1995.

Ogura, Y. and H.-R. Cho, Diagnostoc determination of cumulus populations from large-scale variables, *J. Atmos. Sci., 30*, 1276–1286, 1973

Pickering, K.E., A.M. Thompson, Y. Wang, W.-K. Tao, D.P. McNamara, V.W.J.H. Kirchhoff, B.G. Heikes, G.W. Sachse, J.D. Bradshaw, G.L. Gregory, and D.R. Blake, Convective transport of biomass burning emissions over Brazil during TRACE A, *J. Geophys. Res.,* 101, 23,993–24,012, 1996.

Pickering, K.E., Y. Mang, W.-K. Tao, C. Price, and J.-F. Müller, Vertical distribution of lightning NO_x for use in regional and global chemical transport models, *J. Geophys. Res.,* , 103, 31203–31216, 1998.

Prather, M.J., and D.J. Jacob, A persistent imbalance in HO_x and NO_x photochemistry of the upper troposphere driven by deep tropical convection, *Geophys. Res. Lett., 24*, 3189-3192, 1997.

Rodhe, H., Human impact on the atmospheric sulfur balance, *Tellus, 51,* 110-122, 1999.

Scala, J.R., et al., Cloud draft structure and trace gas transport, *J. Geophys. Res.,* 95, 17,015–17,030, 1990.

Singh, H.B., M. Kanakidou, P.J. Crutzen, and D.J. Jacob, High concentrations and photochemical fate of oxygenated hydrocarbons in the global troposphere, *Nature, 378*, 50-54, 1995.

Snider, J.R., and J. Huang, Factors influencing the retention of hydrogen peroxide and molecular oxygen in rime ice, *J. Geophys. Res., 103*, 1405–1415, 1998.

Thompson, A.M., W.-K. Tao, K.E. Pickering, J.R. Scala, and J. Simpson, Tropical deep convection and ozone formation, *Bull. Am. Meteorol. Soc., 78,* 1043–1054, 1997.

Thornton, D.C., A.R. Bandy, B.W. Blomquist, J.D. Bradshaw and, D.R. Blake, Vertical transport of sulfur dioxide and dimethyl sulfide in deep convection and its role in new particle formation, *J. Geophys. Res., 102,* 28,501–28,509, 1997.

Voisin, D., M. Legrand and N. Chaumerliac, Scavenging of acidic gases (HCOOH, CH_3COOH, HNO_3, HCl and SO_2) and ammonia in mixed liquid-solid water clouds at the Puy de Dôme mountain (France), *J. Geophys. Res.,* , 105, 6817–6835, 2000.

Wang, C., and J.S. Chang, A three-dimensional numerical model of cloud dynamics, microphysics and chemistry, 3. Redistribution of pollutants, *J. Geophys. Res., 98*, 16,787–16,798, 1993.

P. Bechtold and C. Mari, Laboratoire d'Aérologie, UMR 5560 CNRS/Université Paul Sabatier, Toulouse, F-31400, France. (e-mail: marc@aero.obs-mip.fr)

D. J. Jacob, Division of Engineering and Applied Science, Harvard University, Cambridge, MA 02138.

(Received February 4, 2000; revised March 22, 2000; accepted March 28, 2000.)